

Monte Carlo study of cuprate superconductors in a four-band d - p model: Role of orbital degrees of freedom

Hiroshi Watanabe^{1,*}, Tomonori Shirakawa^{2,3}, Kazuhiro Seki³, Hirofumi Sakakibara^{4,5,6}, Takao Kotani^{4,5}, Hiroaki Ikeda⁷, and Seiji Yunoki^{2,3,6,8}

¹*Research Organization of Science and Technology, Ritsumeikan University, Shiga 525-8577, Japan*

²*Computational Materials Science Research Team,*

RIKEN Center for Computational Science (R-CCS), Hyogo 650-0047, Japan

³*Quantum Computational Science Research Team,*

RIKEN Center for Quantum Computing (RQC), Saitama 351-0198, Japan

⁴*Advanced Mechanical and Electronic System Research Center (AMES),*

Faculty of Engineering, Tottori University, Tottori 680-8552, Japan

⁵*Center of Spintronics Research Network (CSRN),*

Graduate School of Engineering Science, Osaka University, Osaka, 560-8531, Japan

⁶*Computational Condensed Matter Physics Laboratory,*

RIKEN Cluster for Pioneering Research (CPR), Saitama 351-0198, Japan

⁷*Department of Physics, Ritsumeikan University, Shiga 525-8577, Japan*

⁸*Computational Quantum Matter Research Team,*

RIKEN Center for Emergent Matter Science (CEMS), Saitama 351-0198, Japan

(Dated: March 16, 2023)

Understanding the various competing phases in cuprate superconductors is a long-standing challenging problem. Recent studies have shown that orbital degrees of freedom, both Cu e_g orbitals and O p orbitals, are a key ingredient for a unified understanding of cuprate superconductors, including the material dependence. Here we investigate a four-band d - p model derived from the first-principles calculations with the variational Monte Carlo method, which allows us to elucidate competing phases on an equal footing. The obtained results can consistently explain the doping dependence of superconductivity, antiferromagnetic and stripe phases, phase separation in the underdoped region, and also novel magnetism in the heavily-overdoped region. The presence of p orbitals is critical to the charge-stripe features, which induce two types of stripe phases with s' -wave and d -wave bond stripe. On the other hand, the presence of d_{z^2} orbital is indispensable to material dependence of the superconducting transition temperature (T_c), and enhances local magnetic moment as a source of novel magnetism in the heavily-overdoped region as well. These findings beyond one-band description could provide a major step toward a full explanation of unconventional normal state and high T_c in cuprate superconductors.

Keywords: superconductivity, cuprates, electron correlation, variational Monte Carlo method, first-principles calculation

I. INTRODUCTION

Over 35 years since its discovery [1], cuprate superconductors have continuously challenged our conventional understandings, such as the recent discovery of nematic transitions in the pseudogap region [2]. It has not yet been achieved to consistently explain the whole phase diagram and the correlation between competing orders and the high transition temperature (T_c). The key to explain the features is considered to be multiorbital effects. The importance of the orbital degrees of freedom is of great interest in modern condensed matter physics as a source of emergent phenomena such as spin currents [3, 4] and, in the field of superconductivity, as a source of novel pairing states and high T_c [5, 6].

In cuprate superconductors, for a long time, the anomalous features have been investigated as the physics of an effective single band crossing a Fermi surface [7] rather than multiorbital effects. The effective one-band models, such as the Hubbard model and the t - J model, successfully predicted d -wave superconductivity, but were insufficient to describe the material dependence of T_c and the unconventional competing orders. The d - p model or the Emery model [8], which consists of Cu $d_{x^2-y^2}$ orbital and O p_x/p_y orbitals, was studied early on as a model involving the multiorbital effect. These models have been intensively studied in terms of the material dependence of T_c , pseudogap phenomena, stripe features, and so on [9–35]. Although these models have partially captured the unconventional features, it could not fully explain the anomalous features of cuprates. For example, the large difference in T_c between ~ 40 K for a La-based system and ~ 90 K for a Hg-based system remained unclear. Recently, one of the authors, Sakakibara and co-authors suggested the importance of the d_{z^2} orbital based on the analysis of a two-orbital model [36]. The importance of the d_{z^2} orbital has also been supported by the latest angle-resolved photoemission spectroscopy experiment [37].

* h-watanb@fc.ritsumei.ac.jp

These studies indicate that both p - and d -orbital degrees of freedom should be properly taken into account for the understanding of cuprate superconductors. In the previous work, we have proposed a four-band d - p model composed of the Cu $d_{x^2-y^2}$ and d_{z^2} orbitals and the O p_x and p_y orbitals as a minimal model to obtain the unified description of cuprate superconductors [38]. On the basis of the variational Monte Carlo (VMC) method, we have shown that this model explains well two key factors about the material dependence of T_c : the contribution of the Cu d_{z^2} orbital to the Fermi surface and the site-energy difference Δ_{dp} between the Cu $d_{x^2-y^2}$ and O p orbitals [39].

In this paper, we investigate the four-band d - p model with the VMC method in more detail. We take the La_2CuO_4 and $\text{HgBa}_2\text{CuO}_4$ systems as typical examples, and especially, elucidate the competing orders of superconductivity, antiferromagnetic (AF) and stripe phases, phase separation in the underdoped region, and novel magnetism in the heavily-overdoped region.

Our major findings are as follows. First, charge/spin stripe state is stable over a wide doping range, and its period decreases as the hole doping rate x increases. At $x = 1/8$, we obtain the same stripe phase as observed experimentally, which is extremely robust in the La-based system, but fragile in the Hg-based system. The AF phase is confined to a narrow doping range near $x \sim 0$. In the underdoped region $0 < x < 1/8$, the phase separation (PS) occurs between the AF and the $x = 1/8$ stripe phase. Suppression of the AF correlation by finite inter-site d - d repulsion causes the transition to a d -wave bond stripe observed in non-La-based systems. Second, concerning the superconductivity, the material dependence of the T_c dome as a function of x is consistently explained. The dome shape is shown to be strongly correlated with whether the undoped AF insulator is Slater- or Mott-type. Finally, we show that novel magnetism observed in the heavily-overdoped region comes from the development of Cu local moments via the Hund's coupling due to the rapid increase of d_{z^2} component with doping.

The rest of this paper is organized as follows. In Sec. II, we introduce the model and the numerical method used in this paper. The four-band d - p model on the two-dimensional square lattice is introduced in Sec. II A. The VMC method and the Gutzwiller-Jastrow type trial wave function are explained in Sec. II B. The tight-binding energy bands for the La_2CuO_4 and $\text{HgBa}_2\text{CuO}_4$ systems, obtained on the basis of the first-principles calculation, are shown in Sec. II C. The numerical results are provided in Sec. III. The energy competition between AF and stripe phases are studied in detail and the ground state phase diagram including the PS is shown in Sec. III A. The symmetry change within the stripe phase is also discussed. The material and Coulomb interaction dependence of superconductivity is shown in Sec. III B through the behavior of superconducting correlation functions. The difference between La- and Hg-based systems is discussed from the band structure and electron correlation

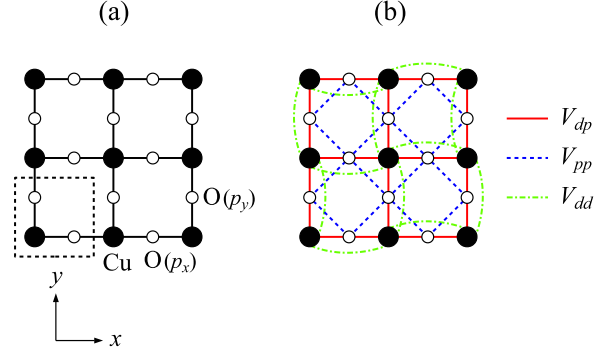


FIG. 1. (a) Lattice structure of the four-band d - p model on the two-dimensional square lattice. There are $d_{x^2-y^2}$ and d_{z^2} orbitals on Cu sites, while there is either p_x or p_y orbital on O sites. Primitive translation vectors $|\mathbf{e}_x| = |\mathbf{e}_y| = 1$ correspond to the lattice constant between the nearest-neighbor Cu sites. The dotted square represents a unit cell. (b) The Coulomb interaction parameters between nearest-neighbor orbitals.

effects. The behavior of d_{z^2} hole density and the local magnetic moment is studied in Sec. III C. The novel magnetism in the heavily-overdoped region is also discussed. Finally, the paper concludes with a summary in Sec. IV. The details of the variational wave functions are shown in Appendix .

II. MODEL AND METHOD

A. Four-band d - p model

As mentioned in Introduction, it is important to incorporate the four orbitals, the Cu e_g orbitals and the O p_x/p_y orbitals, to provide a unified description of the cuprate superconductors. Therefore, we consider a four-band d - p model on the two-dimensional square lattice [see Fig. 1(a)] defined by the following Hamiltonian:

$$H = H_{\text{kin}} + H_{\text{int}} - H_{\text{dc}}. \quad (1)$$

First, the kinetic term H_{kin} is described by

$$H_{\text{kin}} = \sum_{i,j,\sigma} \sum_{\alpha,\beta} t_{ij}^{\alpha\beta} c_{i\alpha\sigma}^\dagger c_{j\beta\sigma} \quad (2)$$

$$= \sum_{\mathbf{k},\sigma} \sum_m E_m(\mathbf{k}) a_{\mathbf{k}m\sigma}^\dagger a_{\mathbf{k}m\sigma}, \quad (3)$$

where Eq. (2) is the kinetic term in an orbital representation and Eq. (3) is in a band representation. $c_{i\alpha\sigma}^\dagger$ ($c_{i\alpha\sigma}$) is a creation (annihilation) operator of an electron at site i with spin σ ($=\uparrow, \downarrow$) and orbital α ($= 1, 2, 3, 4$) corresponding to $(d_{x^2-y^2}, d_{z^2}, p_x, p_y)$, respectively. $t_{ij}^{\alpha\beta}$ denotes a hopping integral between orbital α at site i and orbital β at site j . $t_{ii}^{\alpha\alpha} = \varepsilon_\alpha$ is a site energy for orbital α at site i . These hopping integrals and site energies are determined from the first-principles calculations

(see Sec. II C). $a_{\mathbf{k}m\sigma}^\dagger$ ($a_{\mathbf{k}m\sigma}$) is a creation (annihilation) operator with the wave vector \mathbf{k} , the energy band index m ($= 1, 2, 3, 4$), and spin σ . $E_m(\mathbf{k})$ is a corresponding energy eigenvalue.

Second, the Coulomb interaction term H_{int} is composed of eight terms,

$$\begin{aligned}
 H_{\text{int}} = & U_d \sum_i \left(n_{i\uparrow}^{d_1} n_{i\downarrow}^{d_1} + n_{i\uparrow}^{d_2} n_{i\downarrow}^{d_2} \right) + \left(U'_d - \frac{J}{2} \right) \sum_i n_i^{d_1} n_i^{d_2} \\
 & - 2J \sum_i \mathbf{S}_i^{d_1} \cdot \mathbf{S}_i^{d_2} - J' \sum_i \left(c_{i1\uparrow}^\dagger c_{i1\downarrow}^\dagger c_{i2\uparrow} c_{i2\downarrow} + c_{i2\uparrow}^\dagger c_{i2\downarrow}^\dagger c_{i1\uparrow} c_{i1\downarrow} \right) \\
 & + U_p \sum_i \left(n_{i\uparrow}^{p_x} n_{i\downarrow}^{p_x} + n_{i\uparrow}^{p_y} n_{i\downarrow}^{p_y} \right) \\
 & + V_{dp} \sum_{\langle i,j \rangle} n_i^d n_j^{p_x/y} + V_{pp} \sum_{\langle i,j \rangle} n_i^{p_x} n_j^{p_y} + V_{dd} \sum_{\langle i,j \rangle} n_i^d n_j^d.
 \end{aligned} \tag{4}$$

Here, $n_i^\alpha = n_{i\uparrow}^\alpha + n_{i\downarrow}^\alpha$ with $n_{i\alpha\sigma}^\dagger = c_{i\alpha\sigma}^\dagger c_{i\alpha\sigma}$ is the number operator and \mathbf{S}_i^α is the spin angular momentum operator at site i with orbital α . d_1 and d_2 are abbreviations for $d_{x^2-y^2}$ and d_{z^2} orbitals, respectively, and $n_i^d = n_i^{d_1} + n_i^{d_2}$. U_d, U'_d, J , and J' represent on-site intraorbital, interorbital, Hund's coupling, and pair-hopping interactions between d orbitals, respectively. In this study, we set $J' = J$ and $U_d = U'_d + 2J$ [40]. U_p is the on-site Coulomb interaction of p orbitals. V_{dp}, V_{pp} , and V_{dd} are intersite Coulomb interactions between nearest-neighbor orbitals [see Fig. 1(b)], where the sum $\sum_{\langle i,j \rangle}$ represents nearest-neighbor orbitals located at site i and j . These Coulomb interactions are estimated from the first-principles calculations (see Sec. II C).

Finally, the double counting correction term H_{dc} is introduced,

$$\begin{aligned}
 H_{\text{dc}} = & \left[\left\{ U_d + 2 \left(U'_d - \frac{J}{2} \right) + 16V_{dd} \right\} \bar{n}^d + 8V_{dp} \bar{n}^p \right] \sum_i n_i^d \\
 & + \left\{ (U_p + 8V_{pp}) \bar{n}^p + 8V_{dp} \bar{n}^d \right\} \sum_i (n_i^{p_x} + n_i^{p_y}),
 \end{aligned} \tag{5}$$

where \bar{n}^d and \bar{n}^p are the average electron densities of the d and p orbitals per spin per orbital obtained from the first-principles calculation. This term is subtracted from the Hamiltonian to correct the energy shift that has already been included in the first-principles calculation. In the d - p model, this double counting correction is important to obtain a reasonable result [41].

B. VMC method

In general, it is very difficult to treat the effect of Coulomb interactions correctly. Here, the VMC method [42–44] is employed as a powerful computational method. A Gutzwiller-Jastrow type wave function is considered as a trial state,

$$|\Psi\rangle = P_G^{(2)} P_{J_c} P_{J_s} |\Phi\rangle. \tag{6}$$

$|\Phi\rangle$ is a one-body part obtained by diagonalizing the one-body Hamiltonian including many variational parameters and filling the eigen states in ascending order to the corresponding electron density. The chemical potential is determined in this process. We can construct long-range-ordered states of charge, spin, and superconductivity. The explicit forms of them are described in Appendix.

The Gutzwiller factor

$$P_G^{(2)} = \prod_{i,\gamma} [e^{-g_\gamma} |\gamma\rangle \langle \gamma|_i] \tag{7}$$

is the one extended for the two-orbital system [45, 46]. In $P_G^{(2)}$, possible 16 patterns of charge and spin configuration of the $d_{x^2-y^2}$ and d_{z^2} orbitals at each site $|\gamma\rangle$, i.e., $|0\rangle = |0\ 0\rangle$, $|1\rangle = |0\ \uparrow\rangle$, \dots , $|15\rangle = |\uparrow\downarrow\ \uparrow\downarrow\rangle$, are differently weighted with e^{-g_γ} and $\{g_\gamma\}$ are optimized as variational parameters. The remaining operators

$$P_{J_c} = \exp \left[- \sum_{i,j} \sum_{\alpha,\beta} v_{ij\alpha\beta}^c n_i^\alpha n_j^\beta \right] \tag{8}$$

and

$$P_{J_s} = \exp \left[- \sum_{i,j} \sum_{\alpha,\beta} v_{ij\alpha\beta}^s s_{i\alpha}^z s_{j\beta}^z \right] \tag{9}$$

are charge and spin Jastrow factors, which control long-range charge and spin correlations, respectively. α and β run over four orbitals. $s_{i\alpha}^z$ is the z component of the spin angular momentum operator at site i with orbital α . The set of $\{v_{ij\alpha\beta}^c\}$ and $\{v_{ij\alpha\beta}^s\}$ are variational parameters. The variational parameters in $|\Psi\rangle$ are simultaneously optimized using stochastic reconfiguration method [47]. Antiperiodic boundary conditions are imposed on the x - and y -directions of the primitive lattice vectors.

C. Band structures

We study the La_2CuO_4 and $\text{HgBa}_2\text{CuO}_4$ systems as typical examples of single-layer hole-doped cuprates. The maximally localized Wannier orbitals [48, 49] are constructed from the local-density approximation (LDA) with `ecalj` package [50]. The hopping integrals t_i ($i = 1 - 6$) and the site energy of each orbital ε_α are determined to fit the obtained band structure. They are listed in Table I and the explicit form of the tight-binding model is shown in Appendix 1. Note that $\varepsilon_{d_{z^2}}$ for the La-based system is corrected to a lower value with reference to the quasiparticle self-consistent *GW* (QSGW) method [53–56], which gives realistic correction to the LDA. We have checked its validity in our previous study [38].

Figure 2 shows the noninteracting tight-binding energy bands for La- and Hg-based systems. We can summarize the difference between them as follows. (i) The density of states (DOS) of the d_{z^2} component is extended from -1 to

TABLE I. The tight-binding parameters for the La_2CuO_4 and $\text{HgBa}_2\text{CuO}_4$ systems in eV units. The definitions of t_i and ε_α are described in Appendix 1.

	t_1	t_2	t_3	t_4	t_5	t_6	$\varepsilon_{d_{x^2-y^2}}$	$\varepsilon_{d_{z^2}}$	$\varepsilon_{p_{x/y}}$
La	1.42	0.61	0.07	0.51	0.03	0.07	-0.87	-0.68	-3.13
Hg	1.26	0.65	0.13	0.33	0.00	0.05	-1.41	-1.68	-3.25

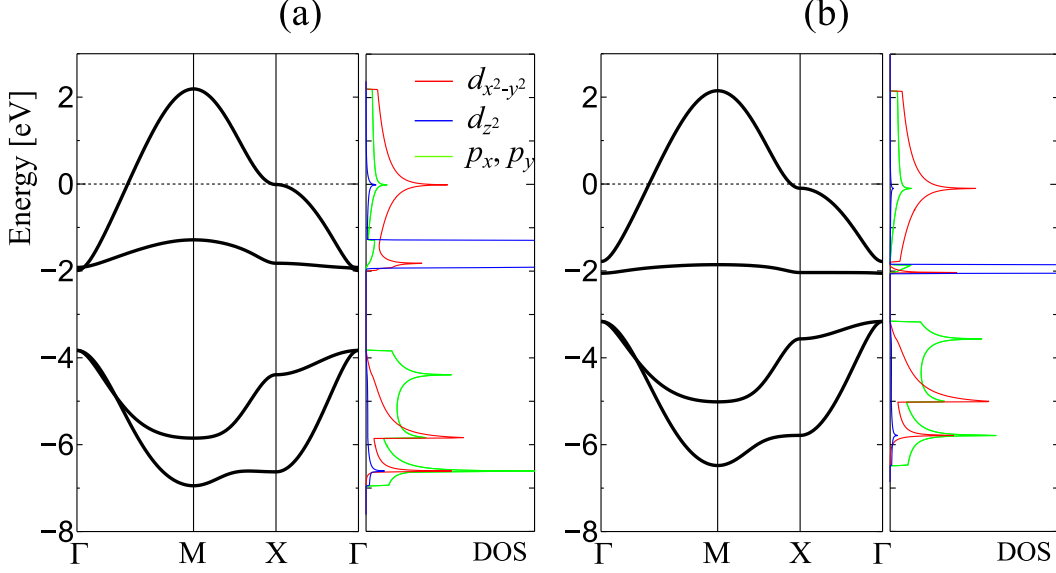


FIG. 2. The energy dispersions of the noninteracting tight-binding models for (a) La_2CuO_4 and (b) $\text{HgBa}_2\text{CuO}_4$ systems. The projected density of states onto four orbitals are also shown. Fermi energies correspond to the 15% hole doping ($x=0.15$). The high symmetric momenta are indicated as $\Gamma = (0, 0)$, $M = (\pi, \pi)$, and $X = (\pi, 0)$.

-2 eV in the La-based system [Fig. 2(a)], while it is almost localized around -2 eV in the Hg-based system [Fig. 2(b)]. In addition, a small but finite peak structure of the d_{z^2} component exists around the Fermi energy (0 eV) in the La-based system, which greatly affects the stability of superconductivity. (ii) The site-energy difference $\Delta_{dp} = \varepsilon_{d_{x^2-y^2}} - \varepsilon_p$ is larger in the La-based system (2.26 eV) than in the Hg-based system (1.84 eV). It affects the strength of the electron correlation through the difference in orbital occupancy. The small Δ_{dp} in the Hg-based system leads to a weaker electron correlation because of the more weight of the $p_{x/y}$ orbital.

Starting from these energy band structures, we will investigate the ground state property of the La- and Hg-based systems using the VMC method. In the following, we set t_1 as a unit of energy. The d -orbital on-site Coulomb interaction U_d/t_1 is varied as a parameter. The other Coulomb interaction parameters are set as $(U'_d, J, U_p, V_{dp}, V_{pp}) = (0.8, 0.1, 0.5, 0.25, 0.2) U_d$ for both La- and Hg-based systems with reference to Ref. [57], unless otherwise noted. We first set $V_{dd} = 0$ and then discuss the effect of finite V_{dd} in Sec. III A 3.

III. RESULTS

The results obtained are presented in three parts, A. AF and Stripe phases, B. Superconductivity, and C. Heavily-overdoped region. In VMC calculations, charge ordering and magnetic ordering generally tend to be more stable than superconductivity. This can be due to insufficient incorporation of quantum fluctuations, which is an issue to be addressed in the future. Instead, the discussion here focuses on the doping and material dependence of each phase. The effect of randomness is out of the scope of this paper. We show results for $N_S = L \times L = 24 \times 24 = 576$ unit cells (and thus $576 \times 4 = 2304$ orbitals in total), which is large enough to avoid finite-size effects.

A. AF and Stripe phases

In this paper, the stripe phase with charge and spin periodicity λ_c and λ_s is denoted as a $C\lambda_c S\lambda_s$ phase according to the convention. For example, the most familiar stripe phase observed around $x = 1/8$ in several La-based systems corresponds to the C4S8 phase. Our

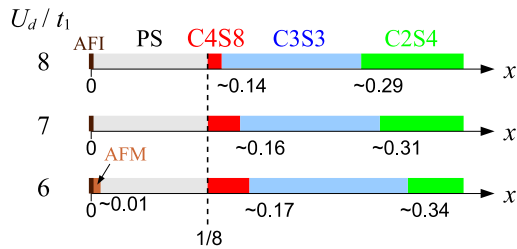


FIG. 3. Ground state phase diagrams for the La-based system for the hole doping rate x with $U_d/t_1 = 6, 7$, and 8 . AFI, AFM, and PS represent AF insulator, AF metal, and phase separation, respectively. $\text{C}\lambda_c\text{S}\lambda_s$ represents the stripe phase with charge and spin periodicity λ_c and λ_s , respectively.

main finding in the charge/spin stripe structure is the “role-sharing” of each orbital; charge modulation occurs mainly on the p_x and p_y orbitals, while spin modulation on the $d_{x^2-y^2}$ orbital. This is because there is an efficient energy gain due to the orbital degrees of freedom, which is an aspect not present in the one-band model. Here we show the energetic competition between AF and stripe phases, and discuss the changes in stripe structures along with the doping and material dependence.

1. La_2CuO_4

Figure 3 depicts the ground-state phase diagram obtained in the La-based system as a function of the hole doping rate x . The AF insulator (AFI) at undoped $x = 0$ readily becomes unstable with doping. For large U_d/t_1 , the AF metallic (AFM) phase does not appear. For $0 < x < 1/8$, the PS occurs between the AFI and the C4S8 stripe phase. Near $x \sim 1/8$, the C4S8 stripe phase is quite stable. The structure of the C4S8 phase is consistent with the experimentally observed $x = 1/8$ stripe structure [58]. The stripe phases are widely observed for $x > 1/8$, although the period of the stripes λ_c decreases monotonically with further doping. In the obtained C3S3 and C2S4 stripe phases, the ground-state energies increase drastically. Unlike the C4S8 phase, these stripe phases have no clear reason for their stabilization and also have never been observed experimentally. We believe that these are artificial states of our VMC calculations, and are in fact liquid-like states due to the thermal/quantum fluctuation. Let us discuss these stripe structure in more detail below.

Figure 4(a) shows ground-state energies of AF and stripe phases as a function of x . One can see that AFI and C4S8 phases are fairly stable. The period of stripe structure λ_c monotonically decreases with x . Although the value of λ_c is limited to an integer value due to commensurability and finite size effects, it will vary smoothly in the limit of infinite system size. For $x < 1/8$, the PS between AFI and C4S8 phases occurs according to the Maxwell construction, and thus

the stripe phase for $\lambda_c > 4$ is a metastable state. The presence of the PS has been reported in previous studies [16, 59–61]. In real materials, the effect of lattice distortion is also important for the stability of the stripe phase. In the La-based systems, such as $\text{La}_{2-x}\text{Sr}_x\text{CuO}_4$ (LSCO), $\text{La}_{2-x}\text{Ba}_x\text{CuO}_4$ (LBCO), and $\text{La}_{2-x-y}\text{Nd}_y\text{Sr}_x\text{CuO}_4$ (LNSCO), the CuO_2 square lattice undergoes a structural transition from a high-temperature tetragonal (HTT) to a low-temperature orthorhombic (LTO) phase. The LTO phase is further deformed to a low-temperature tetragonal (LTT) phase in LBCO and LNSCO. Such structural distortion couples to the stripe phases and stabilizes them. It is possible that some metastable stripe structures in the PS become stable through the structural distortion.

Next, to dissect the stripe structure, we compute the excess energy per added hole [12], $e_h = \frac{E(x) - E(0)}{x}$, and illustrate it in Fig. 4(b) as a function of the stripe filling $\nu = x\lambda_c$. Here, $E(x)$ is the VMC total energy at the hole doping rate x . The stripe filling ν denotes the hole filling of the folded band structure in the stripe phase. For instance, $\nu = 0.5$ and $\nu = 1$ correspond to a half-filled metallic and a fully-filled insulating states, respectively. In Fig. 4(b), one can see that the behavior of e_h is drastically changed around $\lambda_c = 4$. For $\lambda_c > 4$, $\nu = 0.5$ is always stable, especially, the $\lambda_c = 4$ (C4S8) phase observed experimentally is the most stable. This can be the result of maintaining the undoped AFI state as much as possible due to the strong AF correlations, as mentioned in the next paragraph. Note that in our case, the C8S16 phase with $\nu = 1$ proposed in the previous studies does not appear at $x = 1/8$. This phase appears only in peculiar band structures with nearly zero diagonal (next-nearest-neighbor) hopping [12, 61–63]. It is thus not so realistic. On the other hand, for $\lambda_c < 4$, the stable value of ν shifts to smaller values as λ_c decreases. Unlike the stripe structure with $\nu = 0.5$, there is no clear reason for such a stripe structure to be stabilized. In fact, stable stripe phases with $\lambda_c < 4$ have never been observed experimentally for $x > 1/8$. It is natural to assume that such a stripe state is a fluctuating state like a liquid for $x > 1/8$, rather than in a long-range order [64, 65]. More improved calculations incorporating quantum fluctuations can lead to such liquid states [26]. It is important that such short-range correlations develop for $x > 1/8$ [66], which can have significant effects for the mechanism of high- T_c superconductivity.

Next, let us discuss the spin degree of freedom. For all the stripe phases considered here, we find the so-called “spin-charge locking” [58, 67]. Namely, the relation $2\lambda_c = \lambda_s$ ($\lambda_c = \lambda_s$) for even (odd) λ_c is always satisfied. This is because the spin modulation is a driving force of the stripe ordering and the charge modulation only follows it [68]. Indeed, we have checked that the stripe phase without spin modulation, namely, a pure charge stripe phase, is not stabilized within our calculation. Figure 4(c) shows the spin incommensurability δ as a function of x . δ is defined as the difference from the AF

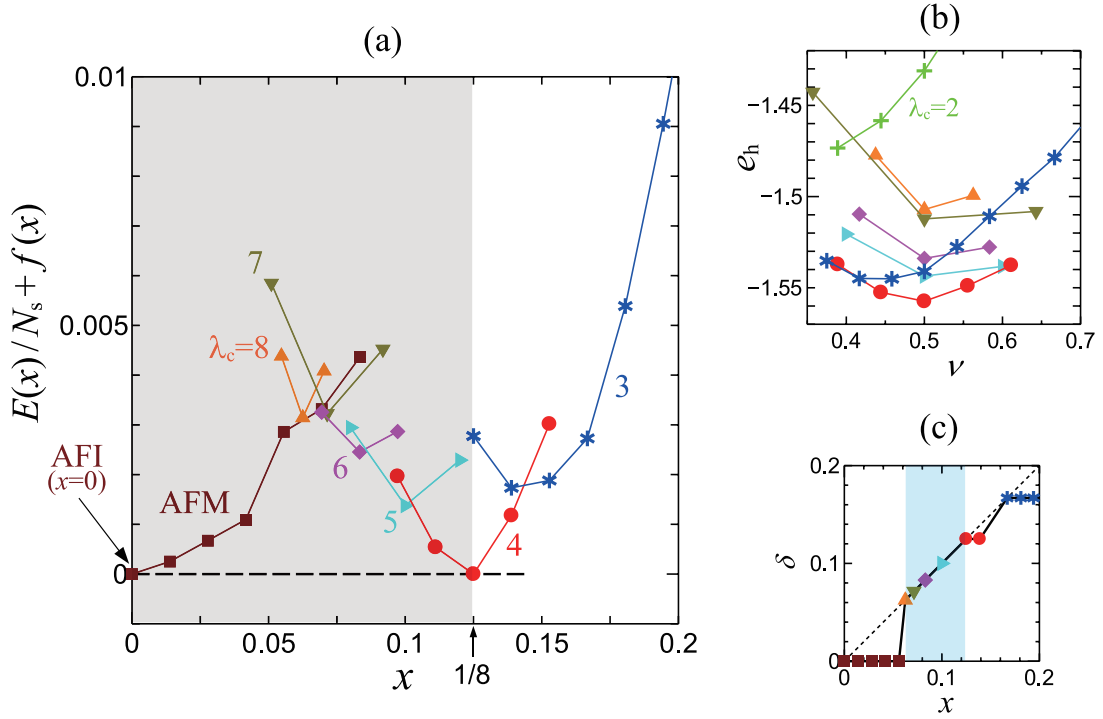


FIG. 4. (a) The x dependence of variational energies per site $E(x)/N_s$ for different phases (AFI, AFM, and stripe phases with charge periodicity λ_c) for the La-based system with $U_d/t_1 = 8$. $f(x) = [-E(0) + 8x\{E(0) - E(1/8)\}]/N_s$ is added for visibility. $t_1 = 1.42$ eV is a unit of energy. $N_s = 24 \times 24$ except for $\lambda_c = 7$ ($N_s = 28 \times 28$) and $\lambda_c = 5$ ($N_s = 20 \times 20$). The dashed line represents the Maxwell construction, which indicates the PS for $0 < x < 1/8$ (gray shaded area). (b) The excess energy per added hole e_h for stripe phase as a function of stripe filling ν . (c) The spin incommensurability δ as a function of x .

wave vector in k_x direction, $\mathbf{k}/2\pi = (\frac{1}{2} \pm \delta, \frac{1}{2})$, where \mathbf{k} is a peak position of the spin structure factor of the stripe phase. In the stripe phases for $\lambda_c \geq 4$, $\delta = x$ is satisfied [blue shaded area for $1/16 \leq x \leq 1/8$ in Fig. 4(c)], which is consistent with “Yamada relation” for the La-based system confirmed in neutron scattering experiments [69]. This implies that the stripe phases with $\lambda_c \geq 4$ are realized. We obtain the relation $\delta = x = 1/\lambda_s$ ($1/2\lambda_s$) for even (odd) λ_c from these stripe filling $\nu = x\lambda_c = 0.5$ and the spin-charge locking. These results suggest that the origin of the stripe phase in the La-based system is not a band (nesting) effect but a strong correlation effect. Actually, it has been reported that λ_c expected from the Fermi-surface nesting has opposite x dependence (λ_c increases with increasing x) [70].

2. $\text{HgBa}_2\text{CuO}_4$

Figure 5 shows the ground state phase diagram of the Hg-based system. Unlike the La-based system, the AFM phase appears in the low-doping region and the PS region is narrower. As shown in Fig. 6(a), the energy of several metastable stripe phases in the PS region is comparable. Although the excess energy per added hole, e_h , for $\lambda_c \geq 4$ has the minimum at $\nu = 0.5$, the energy curve is somewhat shallow compared to the La-based system, as shown

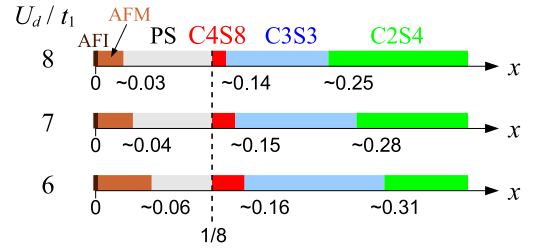


FIG. 5. Ground state phase diagrams for the Hg-based system with $U_d/t_1 = 6, 7$, and 8 . Notation is the same as in Fig. 3.

in Fig. 6(b). Therefore, the half-filled stripe phases are not so robust as in the case of La-based system. This implies that the relation $\delta = x$ for incommensurability [blue shaded area in Fig. 6(c)] is fragile. In fact, no such relationship has been observed experimentally in the Hg-based systems. The stripe phases for $x > 1/8$ is almost the same as in the La-based system.

3. Internal structure of stripe phases and the effect of V_{dd}

Next, let us consider the internal structure of the stripe phases. Figure 7(a) shows the obtained C4S8 structure. Reflecting that the cuprates are the charge-transfer in-

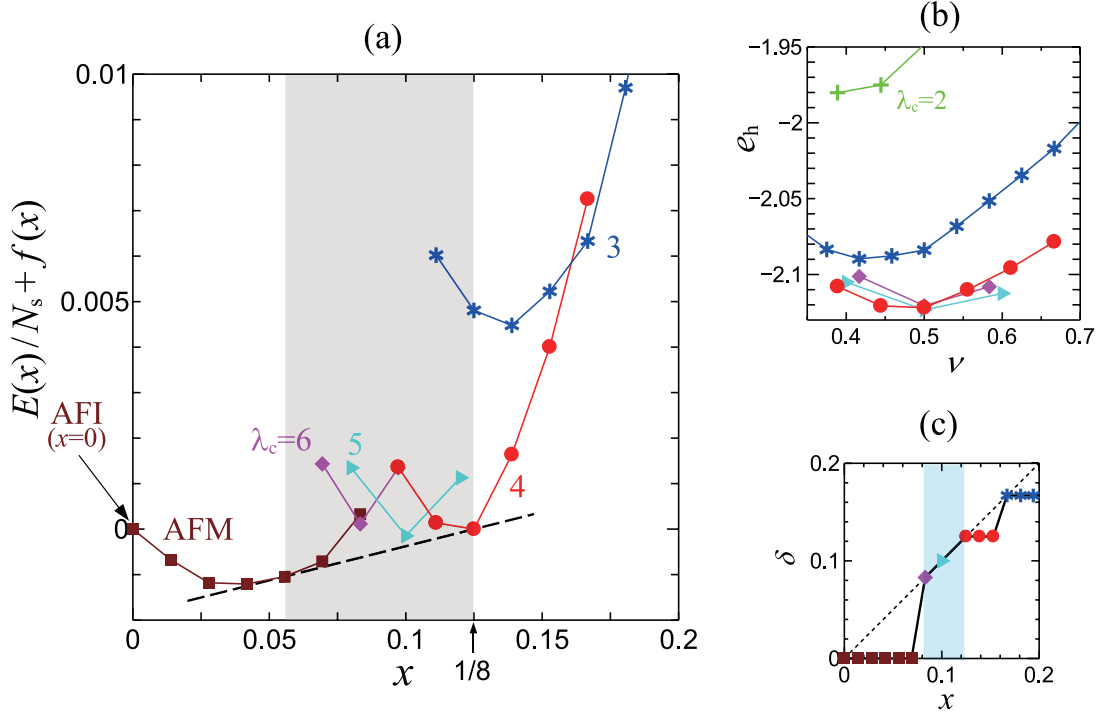


FIG. 6. (a) The x dependence of variational energies per site $E(x)/N_s$ for different phases (AFI, AFM, and stripe phases with charge periodicity λ_c) for the Hg-based system with $U_d/t_1 = 6$. $f(x) = [-E(0) + 8x\{E(0) - E(1/8)\}]/N_s$ is added for visibility. $t_1 = 1.26$ eV is a unit of energy. $N_s = 24 \times 24$ except for $\lambda_c = 5$ ($N_s = 20 \times 20$). The dashed line represents the Maxwell construction, which indicates the PS for $0.06 < x < 1/8$ (gray shaded area). (b) The excess energy per added hole e_h for stripe phase as a function of stripe filling ν . (c) The spin incommensurability δ as a function of x .

ulators, doped hole carriers are mainly introduced into the p orbitals, and the occupation number of the d orbitals remains almost unchanged. Thus, in Fig. 7, only the spin density is depicted for the d orbitals, while only the hole density is depicted for the p orbitals. As can be seen in Fig. 7(a), the charge-density wave (CDW) of the doped hole carriers introduced into the p_x and p_y orbitals appears in-phase. This structure is actually the same as the s' -wave bond-order CDW observed in the La-based systems by the resonant soft X-ray scattering experiment [71]. For the spin density, the spin-rich Cu sites are surrounded by the hole-poor O sites, and vice versa. The system efficiently gains the exchange (kinetic) energy around the hole-poor (hole-rich) sites with this configuration. In this way, spin-active and charge-active areas alternate in a stripe pattern as shown in Fig. 7(a). The observation of the s' -wave CDW is consistent with a slave-boson mean-field approximation [12] and a density-matrix-renormalization-group study [25] on a three-band d - p model.

On the other hand, a stripe structure with an anti-phase CDW of the p orbital in Fig. 7(b) (so-called d -wave CDW) has been proposed for non-La-based systems, such as $\text{Bi}_2\text{Sr}_2\text{CaCu}_2\text{O}_{8+\delta}$ (Bi2212) [72], $\text{Ca}_{2-x}\text{Na}_x\text{CuO}_2\text{Cl}_2$ (Na-CCOC) [72], and $\text{YBa}_2\text{Cu}_3\text{O}_{6+y}$ (YBCO) [73]. In the present calculation, the s' -wave CDW is stable, but the d -wave CDW appears in cases where V_{pp} is a little

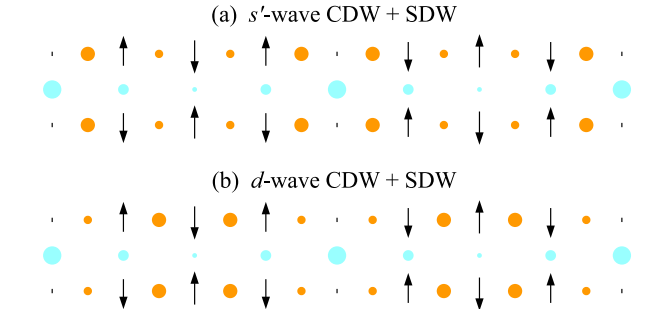


FIG. 7. Schematic pictures of the obtained hole and spin density modulations of the C4S8 phase with (a) s' -wave CDW+SDW and (b) d -wave CDW+SDW. Orange and blue solid circles represent p_x and p_y holes and each radius is proportional to the hole density. Arrows represent the $d_{x^2-y^2}$ spins and each length is proportional to the spin density.

larger, because V_{pp} has a repulsive effect between neighboring p_x and p_y holes and favors the anti-phase CDW. We can also confirm the appearance of the d -wave CDW by introducing a finite V_{dd} , although we have so far assumed $V_{dd} = 0$. As shown in Figs. 8(a) and 8(b), the d -wave CDW is more likely to appear in the moderately correlated Hg-based systems than in the strongly correlated La-based systems, which is consistent with the

experimental results.

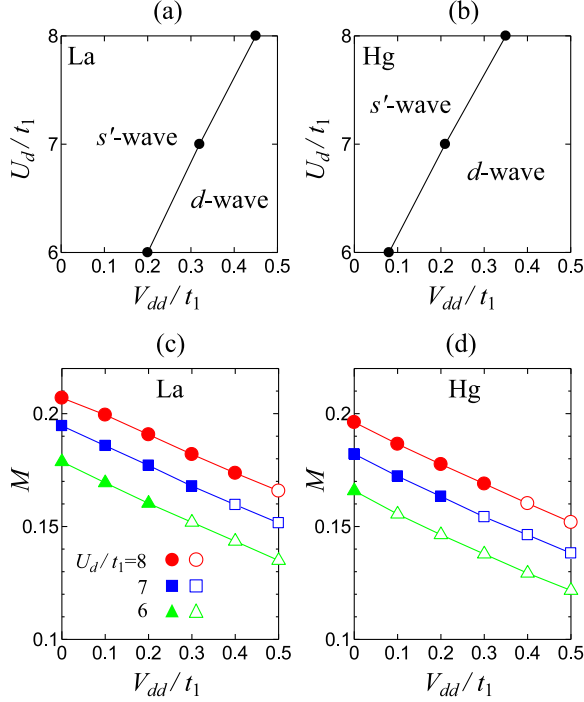


FIG. 8. Internal structure of the C4S8 phase at $x = 56/576 \sim 0.097$ for (a) La-based and (b) Hg-based systems. The order parameter of the SDW in the C4S8 phase, M , for (c) La-based and (d) Hg-based systems. Solid (open) symbols correspond to the s' -(d)-wave CDW+SDW.

In order to clarify the effect of V_{dd} on the stripe, the magnetization in each state,

$$M = \sqrt{\frac{S_z(\mathbf{q}_{\text{peak}})}{N_S}}, \quad (10)$$

is shown in Figs. 8(c) and 8(d), where $S_z(\mathbf{q}_{\text{peak}})$ represents the peak value of the z -component of the $d_{x^2-y^2}$ spin structure factor. With the introduction of V_{dd} , the average magnetization decreases monotonically, and the d -wave CDW appears for $M \lesssim 0.16$. Namely, the introduction of V_{dd} works destructively on the SDW, and eventually the d -wave CDW appears. This is because the V_{dd} effectively weakens U_d by increasing the density of doubly-occupied Cu sites [38], and thus the system becomes less correlated. This situation seems to be a natural connection to the weak correlation approach. Indeed, it has been argued in several theoretical proposals that the d -wave CDW is induced by the nesting effects on the Fermi surface [23, 74, 75]. Since our finite-size calculations have difficulty in capturing the fine structure of the Fermi surfaces, the approach from weak correlations is complementary.

B. Superconductivity

Next let us consider $d_{x^2-y^2}$ -wave spin-singlet superconductivity. Although the coexistence of stripe and superconducting phases is proposed in several cuprates [76–78], here we consider the uniform superconducting phase. The superconducting correlation function is defined as

$$P^{dd}(\mathbf{r}) = \frac{1}{N_S} \sum_i \sum_{\tau, \tau'} f_{\tau\tau'}^{(dd)} \langle \Delta_{\tau}^{\dagger}(\mathbf{R}_i) \Delta_{\tau'}(\mathbf{R}_i + \mathbf{r}) \rangle, \quad (11)$$

where $\Delta_{\tau}^{\dagger}(\mathbf{R}_i)$ is a creation operator of singlet pairs between nearest-neighbor $d_{x^2-y^2}$ orbitals,

$$\Delta_{\tau}^{\dagger}(\mathbf{R}_i) = \frac{1}{\sqrt{2}} (c_{i1\uparrow}^{\dagger} c_{i+\tau 1\downarrow}^{\dagger} + c_{i+\tau 1\uparrow}^{\dagger} c_{i1\downarrow}^{\dagger}), \quad (12)$$

and τ represents four nearest-neighbor Cu sites ($\tau = \pm \mathbf{e}_x, \pm \mathbf{e}_y$). $f_{\tau\tau'}^{(dd)}$ is a form factor of a superconducting gap function with $d_{x^2-y^2}$ symmetry, namely, $f_{\tau\tau'}^{(dd)} = 1$ for $\tau \parallel \tau'$ and -1 for $\tau \perp \tau'$. If $P^{dd}(\mathbf{r})$ is saturated to a finite value for $r = |\mathbf{r}| \rightarrow \infty$, superconducting long-range order exists. In the following, we take the saturated value of $P^{dd}(r \rightarrow \infty)$ as a strength of superconductivity P^{dd} .

The x dependence of P^{dd} for the La-based system is shown in Fig. 9(a). At $x = 0$, the system is an insulator due to correlation effects, and thus superconductivity is completely suppressed, $P^{dd} = 0$. As x increases, the mobility of the Cooper pairs increases due to the introduction of mobile carriers by doping. On the other hand, the strength of the d - d pairing itself is reduced by doping due to the reduction of electron correlation. The former effect is predominant in a low-doping, strongly-correlated region and the latter effect is predominant in a high-doping, weakly-correlated region. In other words, the peak position of the dome corresponds to a boundary between strongly- and weakly-correlated regions. Therefore, the peak position is moved to a smaller value of x with decreasing U_d/t_1 because the weakly-correlated region is extended.

The x dependence of P^{dd} for the Hg-based system is shown in Fig. 9(b). While the dome-shaped behavior is observed for $U_d/t_1 = 7$ and 8, P^{dd} monotonically decreases with x for $U_d/t_1 = 6$. This is because for $U_d/t_1 = 6$, the system is not insulating but metallic at $x = 0$ when the paramagnetic state is assumed. When the AF order is taken into account, the crossover from the Mott insulator to the Slater insulator occurs at $U_d/t_1 \sim 6.3$ in the present model [38]. Namely, the view of a “doped Mott insulator” is no longer valid for $U_d/t_1 = 6$. The shape of P^{dd} can be a measure of the strength of an electron correlation. From this point of view, the La-based system is more strongly correlated than the Hg-based system, because the system is still a Mott insulator at $x = 0$ for $U_d/t_1 = 6$, as shown in Fig. 9(a). It results from the larger value of Δ_{dp} in the La-based system, which leads to a larger d -orbital occupancy of holes and a stronger electron correlation [38].

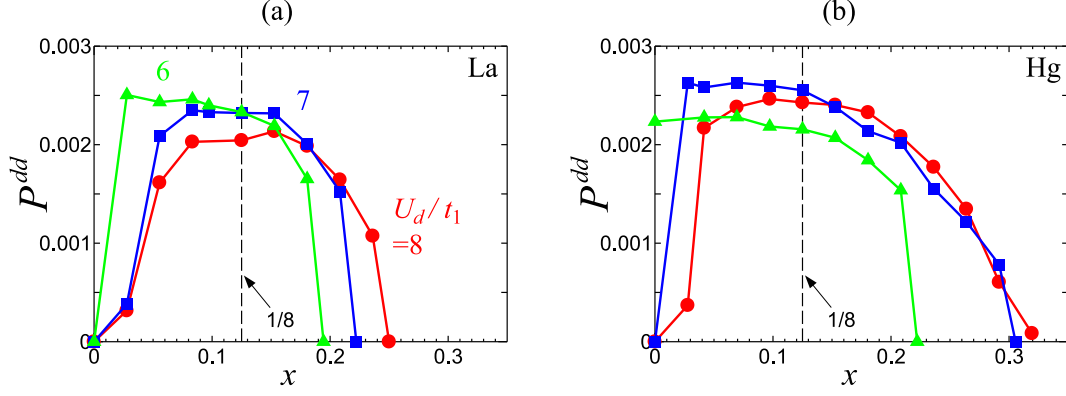


FIG. 9. The x dependence of superconducting correlation function P^{dd} for (a) La-based and (b) Hg-based systems. $N_S = 24 \times 24$.

We can observe that P^{dd} of the Hg-based system is larger than that of the La-based system. It is consistent with the higher T_c in the Hg-based system (~ 90 K) compared with the La-based system (~ 40 K). The reason why P^{dd} of the Hg-based system is larger can be understood as follows: (i) The low $\varepsilon_{d_{z^2}}$ in the Hg-based system is favorable for superconductivity through the less d_{z^2} -orbital contribution to the Fermi surface; the d_{z^2} -orbital contribution to the Fermi surface is destructive for superconductivity due to the localized character of the d_{z^2} electrons [38]. This effect is significant for a high-doping ($x \gtrsim 0.15$) region. (ii) The small $\Delta_{dp}(> 0)$ in the Hg-based system is favorable for superconductivity in a low-doping region ($x \lesssim 0.15$) through the weaker electron correlation due to the hybridization of p orbitals; the electron correlation is destructive for superconductivity in a low-doping region because the mobility of the Cooper pairs is suppressed. P^{dd} itself is a physical quantity in the ground state but is closely related to T_c . We expect that the larger P^{dd} , the higher T_c . We consider that both the band structure and electron correlation effects are necessary to explain the material dependence of T_c .

We also note that the dip structure around $x = 1/8$ becomes slightly more visible as U_d/t_1 increases, in both La-based and Hg-based systems. In fact, the dip structure around $x = 1/8$ is widely observed in cuprate superconductors. This structure is more pronounced the more stable the stripe states are, as in LBCO and LNSCO with the LTT distortion mentioned in Sec. III A 1. The dip structure we found is tightly related to this fact. This implies that although our variational wave functions for the superconductivity do not explicitly include the charge modulation, stripe fluctuations are partially included through the Jastrow factors.

Finally, we mention the finite-size effect. The dome-shaped behavior and the material dependence of P^{dd} are obtained also for $N_S = 16 \times 16$. We consider that $N_S = 24 \times 24$ used here is large enough to discuss the superconductivity in the present model.

C. Heavily-overdoped region

Here, we discuss the hole density of the d_{z^2} orbital n_{z^2} and novel magnetism in the heavily-overdoped region. First of all, in Figs. 10(a) and 10(b), we illustrate n_{z^2} as a function of x for several J/U_d at $U_d/t_1 = 8$ in the La-based and Hg-based systems, along with the superconducting correlation function P_{dd} . In the La-based system, n_{z^2} increases almost linearly with x , and is strongly enhanced by the Hund's coupling J/U_d . Such enhancement of n_{z^2} in the heavily-overdoped region has been also reported by the high-resolution Compton scattering experiment in LSCO [79]. Note that n_{z^2} is suppressed in a finite P_{dd} region. The negative correlation between P_{dd} and n_{z^2} suggests that the d_{z^2} orbital works destructively for superconductivity, which is consistent with the previous studies [36, 38]. Such superconducting-elastic effect could explain the intriguing pressure effect where c -axis compression reduces superconducting T_c [80], because the c -axis compression leads to the increase of n_{z^2} through lowering the apical oxygen height. On the other hand, in the Hg-based system, such an increase of n_{z^2} and suppression of P_{dd} are not so pronounced even at relatively large $J/U_d = 0.2$. This is because the $\varepsilon_{d_{z^2}}$ is much lower in the Hg-based system and the d_{z^2} orbital is almost inactive.

Second, in Figs. 10(c) and 10(d), we show the local moment m_{local} ,

$$m_{\text{local}} = \sqrt{\langle S_i^z S_i^z \rangle} \quad (13)$$

where $S_i^z = \sum_{\alpha} S_{i\alpha}^z$ is the z component of the total spin angular momentum operator at site i and α runs over four orbitals in the unit cell. As shown in Figs. 10(c) and 10(d), m_{local}^2 exhibits quite similar behavior to n_{z^2} . In the La-based system, it suggests that the spin of doped holes in the d_{z^2} orbital is ferromagnetically aligned with that of the $d_{x^2-y^2}$ orbital due to the Hund's coupling, which leads to the increase of m_{local} . Namely, new magnetic "seeds" appear in the heavily-overdoped region originated from the d_{z^2} orbital degree of freedom, which

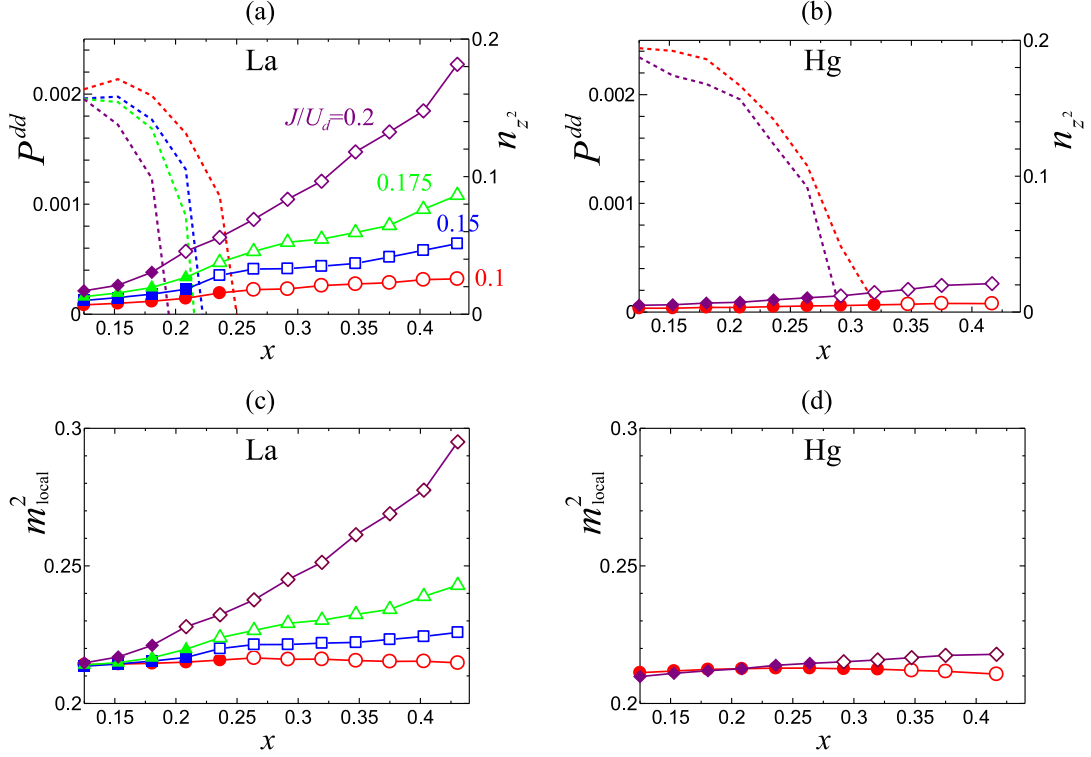


FIG. 10. The x dependence of superconducting correlation function P^{dd} (dotted lines) and the average hole density of the d_{z^2} orbital n_{z^2} (solid lines with symbols) for (a) La-based and (b) Hg-based systems. The x dependence of local moment m_{local} for (c) La-based and (d) Hg-based systems. Solid (open) symbols correspond to the superconducting (paramagnetic) phase. The colors indicate several J/U_d values.

is absent in the one-band Hubbard and even in the three-band d - p models. On the other hand, in the Hg-based system, such a multiorbital effect is not observed because the d_{z^2} orbital is almost inactive. The relative difference in the position of the d_{z^2} orbital causes a clear difference in the doping dependence of the La and Hg systems.

Finally, let us comment a novel magnetism in the heavily-overdoped region. It has been discussed in various ways. Magnetic susceptibility measurements suggest the emergence of local paramagnetic moments in LSCO [81] or ferromagnetic spin fluctuations in $(\text{Bi,Pb})_2\text{Sr}_2\text{CuO}_{6+\delta}$ (Bi-2201) [82, 83]. A zero-field μSR measurement in LSCO also suggests the development of ferromagnetic spin fluctuations [84]. Theoretical studies show the possibility of ferromagnetism using a quantum scaling theory [85], first-principles calculations for supercells of LBCO [86], determinant quantum Monte Carlo [87], dynamical cluster approximation [88], and fluctuation exchange approximation [89]. We can consider two mechanisms for the ferromagnetism in the heavily-overdoped region. One is the band effect. The peak position of the spin susceptibility at $\mathbf{q} = (\pi, \pi)$ in the low-doping region moves toward $\mathbf{q} = (0, 0)$ with hole doping. Indeed, the Lifshitz transition where the topology of the Fermi surface changes from hole-like to electron-like occurs around $x \sim 0.3$ in the one-band Hub-

bard model with $t'/t = -0.3$, leading to the enhancement of $\chi_0(0, 0)$. The other is the multiorbital effect, i.e., the double-exchange mechanism originated from the Hund's coupling between the $d_{x^2-y^2}$ and d_{z^2} orbitals. Our result supports this mechanism. We expect that these two mechanisms will not contradict but rather cooperatively work toward ferromagnetism.

IV. DISCUSSION AND SUMMARY

In this paper, we present a unified explanation of the doping and material dependence of the ground state in cuprate superconductors using the VMC analysis of the four-band d - p model derived from the first-principles calculations. First, we found the following results from a comparison of total energies of the AFI, AFM, and stripe phases. In the Hg-based system, a slight hole-doping causes the appearance of AFM phase, but in the La-based systems, the AFM state is less likely to appear due to strong correlations. In the La-based system, the experimentally observed s' -wave bond stripe phase is quite stable, and all stable stripe structures are in the spin-charge locking state. Overall features of spin incommensurability observed in the neutron scattering experiments are explained. In the Hg-based system, introducing a small

but finite V_{dd} or slightly increasing V_{pp} can lead to a transition to the d -wave bond stripe structure and even a spin-charge unlocked state. PS appears in the low-doping region of both La- and Hg-based systems. All of these behaviors are consistent with experimental observations, and our results generally capture their characteristic features well.

Next, we computed the superconducting correlation functions P^{dd} , and clarified that the dome-shaped P^{dd} , indicative of the T_c dome as a function of the hole doping rate, is originated from the dual nature of the Coulomb repulsion, that is, the enhancement of the pairing interaction and the depairing effect by the decrease of mobile electron pairs. $\varepsilon_{d_{z^2}}$ and Δ_{dp} are material-dependent key parameters for high T_c . Our result suggests that deep $\varepsilon_{d_{z^2}}$ and small Δ_{dp} raise the T_c . This is the reason why T_c of the Hg-based system is higher than that of the La-based system.

Finally, we investigated novel magnetism in heavily-overdoped region. For the hole doping rate $x > 1/8$, both the d_{z^2} hole density n_{z^2} and the local moment at Cu sites increases almost linearly with x in the La-based system. This means that the e_g orbital spins are aligned parallel via the Hund's coupling. These local spins can be ferromagnetically aligned by the double-exchange mechanism, which is consistent with previous proposals. On the other hand, such a multi-orbital effect is not observed in the Hg-based system because the d_{z^2} orbital is located much lower and thus almost inactive.

These findings, which are beyond one-band description, could provide a major step toward a full explanation of unconventional normal state and high- T_c in cuprate superconductors.

ACKNOWLEDGMENTS

The authors thank K. Kuroki, T. Tohyama, and T. Adachi for useful discussions. The computation has been done using the facilities of the Supercomputer Center, Institute for Solid State Physics, University of Tokyo and the supercomputer system HOKUSAI in RIKEN. This work was supported by a Grant-in-Aid for Scientific Research on Innovative Areas “Quantum Liquid Crystals” (KAKENHI Grant No. JP19H05825) from JSPS of Japan, and also supported by JSPS KAKENHI (Grant Nos. JP22K03520, JP22K03512, JP21H04446, JP20K03847, JP19K23433, JP19H01842, and JP18H01183).

Appendix: Construction of the trial wave function

1. Noninteracting energy band

First, we show the construction of the noninteracting tight-binding energy band discussed in Sec. II C. It is obtained by diagonalizing the following one-body Hamiltonian:

$$H_{\text{kin}} = \sum_{\mathbf{k}, \sigma} \begin{pmatrix} c_{\mathbf{k}1\sigma}^\dagger & c_{\mathbf{k}2\sigma}^\dagger & c_{\mathbf{k}3\sigma}^\dagger & c_{\mathbf{k}4\sigma}^\dagger \end{pmatrix} \begin{pmatrix} t_{11} & t_{21}^* & t_{31}^* & t_{41}^* \\ t_{21} & t_{22} & t_{32}^* & t_{42}^* \\ t_{31} & t_{32} & t_{33} & t_{43}^* \\ t_{41} & t_{42} & t_{43} & t_{44} \end{pmatrix} \begin{pmatrix} c_{\mathbf{k}1\sigma} \\ c_{\mathbf{k}2\sigma} \\ c_{\mathbf{k}3\sigma} \\ c_{\mathbf{k}4\sigma} \end{pmatrix} \quad (\text{A.1})$$

$$= \sum_{\mathbf{k}, \sigma} \sum_m E_m(\mathbf{k}) a_{\mathbf{k}m\sigma}^\dagger a_{\mathbf{k}m\sigma} \quad (\text{A.2})$$

with the hopping matrix elements given as

$$t_{11} = \varepsilon_{d_{x^2-y^2}}, \quad (\text{A.3})$$

$$t_{21} = 0, \quad (\text{A.4})$$

$$t_{22} = \varepsilon_{d_{z^2}} - 2t_5(\cos k_x + \cos k_y), \quad (\text{A.5})$$

$$t_{31} = 2it_1 \sin \frac{1}{2}k_x, \quad (\text{A.6})$$

$$t_{32} = -2it_4 \sin \frac{1}{2}k_x, \quad (\text{A.7})$$

$$t_{33} = \varepsilon_{p_x} + 2t_3 \cos k_x + 2t_6[\cos(k_x + k_y) + \cos(k_x - k_y)], \quad (\text{A.8})$$

$$t_{41} = -2it_1 \sin \frac{1}{2}k_y, \quad (\text{A.9})$$

$$t_{42} = -2it_4 \sin \frac{1}{2}k_y, \quad (\text{A.10})$$

$$t_{43} = 2t_2 \left[\cos \left(\frac{1}{2}k_x + \frac{1}{2}k_y \right) - \cos \left(\frac{1}{2}k_x - \frac{1}{2}k_y \right) \right], \quad (\text{A.11})$$

$$t_{44} = \varepsilon_{p_y} + 2t_3 \cos k_y + 2t_6[\cos(k_x + k_y) + \cos(k_x - k_y)], \quad (\text{A.12})$$

where $c_{\mathbf{k}\alpha\sigma}^\dagger$ ($c_{\mathbf{k}\alpha\sigma}$) is a creation (annihilation) operator of an electron with wave vector \mathbf{k} , spin σ ($=\uparrow, \downarrow$), and orbital α ($= 1, 2, 3, 4$) corresponding to ($d_{x^2-y^2}$, d_{z^2} , p_x , p_y), respectively. The hopping integrals t_i ($i = 1 - 6$) and the site energy of each orbital ε_α are determined to fit the band structures obtained from the LDA or QSGW calculation.

2. Trial wave function

a. Superconductivity

To construct the trial wave function for superconductivity, we employ the Bogoliubov de-Gennes (BdG) type Hamiltonian in real space [90], i.e.,

$$H_{\text{BdG}} = \sum_{i,j} \sum_{\alpha,\beta} \begin{pmatrix} c_{i\alpha\uparrow}^\dagger & c_{i\alpha\downarrow} \end{pmatrix} \begin{pmatrix} T_{ij\uparrow}^{\alpha\beta} & \Delta_{ij}^{\alpha\beta} \\ \Delta_{ji}^{\alpha\beta*} & -T_{ji\downarrow}^{\alpha\beta} \end{pmatrix} \begin{pmatrix} c_{j\beta\uparrow} \\ c_{j\beta\downarrow} \end{pmatrix}. \quad (\text{A.13})$$

Here, $T_{ij\sigma}^{\alpha\beta}$ is a normal part and corresponds to the 4×4 matrix in Eq. (A.1) with renormalized hopping integrals \tilde{t}_i and also includes the chemical potential term. The chemical potential μ is set to the corresponding Fermi energy. $\Delta_{ij}^{\alpha\beta}$ is an anomalous part that represents the superconducting pairing in real space. Therefore, the variational parameters to be optimized in $|\Phi\rangle$ are \tilde{t}_i ($i = 2 - 6$) and $\{\Delta_{ij}^{\alpha\beta}\}$ with $\tilde{t}_1 = t_1$ being fixed as a unit of energy. In this study, the pairing between nearest-neighbor orbitals, d - d , d - p_x , d - p_y , p_x - p_x , and p_y - p_y , are considered. d denotes the $d_{x^2-y^2}$ orbital. If we set $\Delta_{ij}^{\alpha\beta} = 0$, the paramagnetic phase is obtained.

b. Uniform spin AF and stripe phases

As mentioned in Sec. II B, various long-range orderings of charge and spin can be described by introducing $\{\rho_i^\alpha\}$ and $\{m_i^\alpha\}$. A uniform spin AF phase along the z - and x -direction can be introduced as

$$m_{(z)}^\alpha \sum_i e^{i\mathbf{Q}\cdot\mathbf{r}_i} \left(c_{i\alpha\uparrow}^\dagger c_{i\alpha\uparrow} - c_{i\alpha\downarrow}^\dagger c_{i\alpha\downarrow} \right) \quad (\text{A.14})$$

and

$$m_{(x)}^\alpha \sum_i e^{i\mathbf{Q}\cdot\mathbf{r}_i} \left(c_{i\alpha\uparrow}^\dagger c_{i\alpha\downarrow} + c_{i\alpha\downarrow}^\dagger c_{i\alpha\uparrow} \right) \quad (\text{A.15})$$

for each orbital α ($= 1, 2, 3, 4$), where $\mathbf{Q} = (\pi, \pi)$, and $m_{(z)}^\alpha$ and $m_{(x)}^\alpha$ are treated as variational parameters. They are energetically degenerate within a one-body description. However, they will give different variational energies with the Gutzwiller and Jastrow factors in Eq. (6) that break the SU(2) symmetry. We have confirmed that $m_{(x)}^\alpha$ always gives a lower variational energy and thus a better trial state. This is because the Gutzwiller and Jastrow factors generate spin fluctuations in the direction orthogonal to that of $m_{(x)}^\alpha$.

For a stripe phase with charge and spin periodicities $\lambda_c^\alpha = 2\pi/q_c^\alpha$ and $\lambda_s^\alpha = 2\pi/q_s^\alpha$, respectively, the following potentials with spatial modulation in the x direction should be introduced at site i for each orbital α ($= 1, 2, 3, 4$):

$$\rho_i^\alpha = \rho^\alpha \cos[q_c^\alpha(x_i - x_c^\alpha)] \quad (\text{A.16})$$

and

$$m_i^\alpha = (-1)^{x_i+y_i} m^\alpha \sin[q_s^\alpha(x_i - x_s^\alpha)], \quad (\text{A.17})$$

where ρ^α and m^α are the amplitude of charge and spin orderings, respectively. x_c^α and x_s^α control the relative

phases of charge and spin orderings, respectively. λ_c^α , λ_s^α , ρ^α , m^α , x_c^α and x_s^α are all variational parameters to be optimized.

-
- [1] Bednorz J G and Muller K A 1986 Possible high- T_c superconductivity in the Ba-La-Cu-O system *Z. Phys. B* **64** 189
 - [2] Sato Y *et al.* 2017 Thermodynamic evidence for a nematic phase transition at the onset of the pseudogap in $\text{YBa}_2\text{Cu}_3\text{O}_y$ *Nat. Phys.* **13** 1074
 - [3] Murakami S, Nagaosa N and Zhang S-C 2003 Dissipationless Quantum Spin Current at Room Temperature *Science* **301** 1348.
 - [4] Kato Y K, Myers R C, Gossard A C and Awschalom D D 2004 Observation of the Spin Hall Effect in Semiconductors *Science* **306** 1910
 - [5] Kuroki K, Onari S, Arita R, Usui H, Tanaka Y, Kontani H and Aoki H 2008 Unconventional Pairing Originating from the Disconnected Fermi Surfaces of Superconducting $\text{LaFeAsO}_{1-x}\text{F}_x$ *Phys. Rev. Lett.* **101** 087004
 - [6] Agterberg D F, Brydon P M R and Timm C 2017 Bogoliubov Fermi Surfaces in Superconductors with Broken Time-Reversal Symmetry *Phys. Rev. Lett.* **118** 127001
 - [7] Damascelli A, Hussain Z and Shen Z-X 2003 Angle-resolved photoemission studies of the cuprate superconductors *Rev. Mod. Phys.* **75** 473
 - [8] Emery V J 1987 Theory of high- T_c superconductivity in oxides *Phys. Rev. Lett.* **58** 2794
 - [9] Asahata T, Oguri A and Maekawa S 1996 Superconducting State in the Three-Band Hubbard Model: A Variational Monte Carlo Study *J. Phys. Soc. Jpn.* **65** 365
 - [10] Takimoto T and Moriya T 1997 Theory of Spin Fluctuation-Induced Superconductivity Based on a $d-p$ Model *J. Phys. Soc. Jpn.* **66** 2459; Takimoto T and Moriya T 1998 Theory of Spin Fluctuation-Induced Superconductivity Based on a $d-p$ Model. II. Superconducting State *ibid.* **67** 3570
 - [11] Yanagisawa T, Koike S and Yamaji K 2001 Ground state of the three-band Hubbard model *Phys. Rev. B* **64** 184509
 - [12] Lorenzana J and Seibold G 2002 Metallic Mean-Field Stripes, Incommensurability, and Chemical Potential in Cuprates *Phys. Rev. Lett.* **89** 136401
 - [13] Shinkai S, Ikeda H and Yamada K 2006 Study of Superconducting Transition Temperature in $d-p$ Model on Basis of Perturbation Theory *J. Phys. Soc. Jpn.* **75** 104712
 - [14] Kent P R C, Saha-Dasgupta T, Jepsen O, Andersen O K, Macridin A, Maier T A, Jarrell M and Schulthess T C 2008 Combined density functional and dynamical cluster quantum Monte Carlo calculations of the three-band Hubbard model for hole-doped cuprate superconductors *Phys. Rev. B* **78** 035132
 - [15] Thomale R and Greiter M 2008 Numerical analysis of three-band models for CuO planes as candidates for a spontaneous T-violating orbital current phase *Phys. Rev. B* **77** 094511
 - [16] Arrigoni E, Aichhorn M, Daghofer M and Hanke W 2009 Phase diagram and single-particle spectrum of CuO_2 high- T_c layers: variational cluster approach to the three-band Hubbard model *New J. Phys.* **11** 055066
 - [17] Weber C, Läuchli A, Mila F and Giamarchi T 2009 Orbital Currents in Extended Hubbard Models of High- T_c Cuprate Superconductors *Phys. Rev. Lett.* **102** 017005
 - [18] Weber C, Haule K and Kotliar G 2010 Strength of correlations in electron- and hole-doped cuprates *Nat. Phys.* **6** 574
 - [19] Weber C, Haule K and Kotliar G 2010 Apical oxygens and correlation strength in electron- and hole-doped copper oxides *Phys. Rev. B* **82** 125107
 - [20] Fischer M H and Kim E-A 2011 Mean-field analysis of intra-unit-cell order in the Emery model of the CuO_2 plane *Phys. Rev. B* **84** 144502
 - [21] Weber C, Yee C, Haule K and Kotliar G 2012 Scaling of the transition temperature of hole-doped cuprate superconductors with the charge-transfer energy *Europhys. Lett.* **100** 37001
 - [22] Bulut S, Atkinson W A and Kampf A P 2013 Spatially modulated electronic nematicity in the three-band model of cuprate superconductors *Phys. Rev. B* **88** 155132
 - [23] Yamakawa Y and Kontani H 2015 Spin-Fluctuation-Driven Nematic Charge-Density Wave in Cuprate Superconductors: Impact of Aslamazov-Larkin Vertex Corrections *Phys. Rev. Lett.* **114** 257001
 - [24] Ogura D and Kuroki K 2015 Asymmetry of superconductivity in hole- and electron-doped cuprates: Explanation within two-particle self-consistent analysis for the three-band model *Phys. Rev. B* **92** 144511
 - [25] White S R and Scalapino D J 2015 Doping asymmetry and striping in a three-orbital CuO_2 Hubbard model *Phys. Rev. B* **92** 205112
 - [26] Huang E W, Mendl C B, Liu S, Johnston S, Jiang H-C, Moritz B and Devereaux T P 2017 Numerical evidence of fluctuating stripes in the normal state of high- T_c cuprate superconductors *Science* **358** 1161
 - [27] Tsuchiizu M, Kawaguchi K, Yamakawa Y and Kontani H 2018 Multistage electronic nematic transitions in cuprate superconductors: A functional-renormalization-group analysis *Phys. Rev. B* **97** 165131
 - [28] Orth P P, Jeevanesan B, Fernandes R M and Schmalian J 2019 Enhanced nematic fluctuations near an antiferromagnetic Mott insulator and possible application to high- T_c cuprates *npj Quantum Mater.* **4** 4
 - [29] Zegrodnik M, Biborski A, Fidrysiak M and Spalek J 2019 Superconductivity in the three-band model of cuprates: Variational wave function study and relation to the single-band case *Phys. Rev. B* **99** 104511
 - [30] Dash S S and Sénéchal D 2019 Pseudogap transition within the superconducting phase in the three-band Hubbard model *Phys. Rev. B* **100** 214509
 - [31] Moreo A and Dagotto E 2019 Minimal-size real-space d -wave pairing operator in CuO_2 planes *Phys. Rev. B* **100** 214502
 - [32] Biborski A, Zegrodnik M and Spalek J 2020 Superconducting properties of the hole-doped three-band $d-p$ model studied with minimal-size real-space d -wave pairing operators *Phys. Rev. B* **101** 214504
 - [33] Cui Z-H, Sun C, Ray U, Zheng B-X, Sun Q and Chan G K-L 2020 Ground-state phase diagram of the three-band

- Hubbard model from density matrix embedding theory *Phys. Rev. Research* **2** 043259
- [34] Chciak A, Vitali E and Zhang S 2020 Magnetic and charge orders in the ground state of the Emery model: Accurate numerical results *Phys. Rev. B* **102** 214512
- [35] Mai P, Balduzzi G, Johnston S and Maier T 2021 Orbital structure of the effective pairing interaction in the high-temperature superconducting cuprates *npj Quantum Mater.* **6** 26
- [36] Sakakibara H, Usui H, Kuroki K, Arita R and Aoki H 2010 Two-Orbital Model Explains the Higher Transition Temperature of the Single-Layer Hg-Cuprate Superconductor Compared to That of the La-Cuprate Superconductor *Phys. Rev. Lett.* **105** 057003
- [37] Matt C E *et al.* 2018 Direct observation of orbital hybridisation in a cuprate superconductor *Nat. Commun.* **9** 972
- [38] Watanabe H, Shirakawa T, Seki K, Sakakibara H, Kotani T, Ikeda H and Yunoki S 2021 Unified description of cuprate superconductors using a four-band d - p model *Phys. Rev. Research* **3** 033157
- [39] Ohta Y, Tohyama T and Maekawa S 1991 Apex oxygen and critical temperature in copper oxide superconductors: Universal correlation with the stability of local singlets *Phys. Rev. B* **43** 2968
- [40] Kanamori J 1963 Electron Correlation and Ferromagnetism of Transition Metals *Prog. Theor. Phys.* **30** 275
- [41] Hansmann P, Parragh N, Toschi A, Sangiovanni G and Held K 2014 Importance of $d - p$ Coulomb interaction for high T_c cuprates and other oxides *New J. Phys.* **16** 033009
- [42] McMillan W L 1965 Ground State of Liquid He^4 *Phys. Rev.* **138** A442
- [43] Ceperley D, Chester G V and Kalos M H 1977 Monte Carlo simulation of a many-fermion study *Phys. Rev. B* **16** 3081
- [44] Yokoyama H and Shiba H 1987 Variational Monte-Carlo Studies of Hubbard Model. I *J. Phys. Soc. Jpn.* **56** 1490
- [45] Bünemann J, Weber W and Gebhard F 1998 Multiband Gutzwiller wave functions for general on-site interactions *Phys. Rev. B* **57** 6896
- [46] Watanabe H, Seki K and Yunoki S 2015 Charge-density wave induced by combined electron-electron and electron-phonon interactions in $1T\text{-TiSe}_2$: A variational Monte Carlo study *Phys. Rev. B* **91** 205135
- [47] Sorella S 2001 Generalized Lanczos algorithm for variational quantum Monte Carlo *Phys. Rev. B* **64** 024512; Yunoki S and Sorella S 2006 Two spin liquid phases in the spatially anisotropic triangular Heisenberg model *ibid.* **74** 014408
- [48] Marzari N and Vanderbilt D 1997 Maximally localized generalized Wannier functions for composite energy bands *Phys. Rev. B* **56** 12847
- [49] Souza I, Marzari N and Vanderbilt D 2001 Maximally localized Wannier functions for entangled energy bands *Phys. Rev. B* **65** 035109
- [50] A first-principles electronic-structure suite based on the plane-wave + muffin-tin orbital (PMT) method [51, 52], ecalj package, is freely available from <https://github.com/tkotani/ecalj>.
- [51] Kotani T and van Schilfgaarde M 2010 Fusion of the LAPW and LMTO methods: The augmented plane wave plus muffin-tin orbital method *Phys. Rev. B* **81** 125117
- [52] Kotani T, Kino H and Akai H 2015 Formulation of the Augmented Plane-Wave and Muffin-Tin Orbital Method *J. Phys. Soc. Jpn.* **84** 034702
- [53] S. V. Faleev, M. van Schilfgaarde, and T. Kotani, All-Electron Self-Consistent GW Approximation: Application to Si, MnO, and NiO, *Phys. Rev. Lett.* **93**, 126406 (2004).
- [54] van Schilfgaarde M, Kotani T and Faleev S V 2006 Quasiparticle Self-Consistent GW Theory *Phys. Rev. Lett.* **96** 226402
- [55] Kotani T, van Schilfgaarde M and Faleev S V 2007 Quasiparticle self-consistent GW method: A basis for the independent-particle approximation *Phys. Rev. B* **76** 165106
- [56] Jang S W, Kotani T, Kino H, Kuroki K and Han M J 2015 Quasiparticle self-consistent GW study of cuprates: electronic structure, model parameters and the two-band theory for T_c *Sci. Rep.* **5** 12050
- [57] Hirayama M, Misawa T, Ohgoe T, Yamaji Y and Imada M 2019 Effective Hamiltonian for cuprate superconductors derived from multiscale *ab initio* scheme with level renormalization *Phys. Rev. B* **99** 245155
- [58] Tranquada J M, Sternlieb B J, Axe J D, Nakamura Y and Uchida S 1995 Evidence for stripe correlations of spins and holes in copper oxide superconductors *Nature* **375** 561
- [59] Emery V J and Kivelson S A 1993 Frustrated electronic phase separation and high-temperature superconductors *Physica C* **209** 597
- [60] Misawa T and Imada M 2014 Origin of high- T_c superconductivity in doped Hubbard models and their extensions: Roles of uniform charge fluctuations *Phys. Rev. B* **90** 115137
- [61] Ido K, Ohgoe T and Imada M 2018 Competition among various charge-inhomogeneous states and d -wave superconducting state in Hubbard models on square lattices *Phys. Rev. B* **97** 045138
- [62] Zheng B-X, Chung C-M, Corboz P, Ehlers G, Qin M-P, Noack R M, Shi H, White S R, Zhang S and Chan G K-L 2017 Stripe order in the underdoped region of the two-dimensional Hubbard model *Science* **358** 1155
- [63] Jiang H-C and Devereaux T P 2019 Superconductivity in the doped Hubbard model and its interplay with next-nearest hopping t' *Science* **365** 1424
- [64] Wen J-J *et al.* 2019 Observation of two types of charge-density-wave orders in superconducting $\text{La}_{2-x}\text{Sr}_x\text{CuO}_4$ *Nat. Commun.* **10** 3269
- [65] von Arx K *et al.* 2022 Fate of charge order in overdoped La-based cuprates arXiv:2206.06695
- [66] Seibold G, Arpaia R, Peng Y Y, Fumagalli R, Braicovich L, Di Castro C, Grilli M, Ghiringhelli G and Caprara S 2021 Strange metal behaviour from charge density fluctuations in cuprates *Commun. Phys.* **4** 7
- [67] Blackburn E *et al.* 2013 X-Ray Diffraction Observations of a Charge-Density-Wave Order in Superconducting Ortho-II $\text{YBa}_2\text{Cu}_3\text{O}_{6.54}$ Single Crystals in Zero Magnetic Field *Phys. Rev. Lett.* **110** 137004
- [68] Tocchio L F, Montorsi A and Becca F 2019 Metallic and insulating stripes and their relation with superconductivity in the doped Hubbard model *SciPost Phys.* **7** 021
- [69] Yamada K *et al.* 1998 Doping dependence of the spatially modulated dynamical spin correlations and the superconducting-transition temperature in $\text{La}_{2-x}\text{Sr}_x\text{CuO}_4$ *Phys. Rev. B* **57** 6165
- [70] Miao H *et al.* 2019 Formation of Incommensurate Charge

- Density Waves in Cuprates *Phys. Rev. X* **9** 031042
- [71] Achkar A J *et al.* 2016 Orbital symmetry of charge-density-wave order in $\text{La}_{1.875}\text{Ba}_{0.125}\text{CuO}_4$ and $\text{YBa}_2\text{Cu}_3\text{O}_{6.67}$ *Nature Mater.* **15** 616
- [72] Fujita K *et al.* 2014 Direct phase-sensitive identification of a d -form factor density wave in underdoped cuprates *Proc. Natl. Acad. Sci. USA* **111** E3026
- [73] Comin R *et al.* 2015 Symmetry of charge order in cuprates *Nature Mater.* **14** 796
- [74] Sachdev S and La Placa R 2013 Bond Order in Two-Dimensional Metals with Antiferromagnetic Exchange Interactions *Phys. Rev. Lett.* **111** 027202
- [75] Efetov K B, Meier H and Pépin C 2013 Pseudogap state near a quantum critical point *Nature Phys.* **9** 442
- [76] Hamidian M H *et al.* 2016 Detection of a Cooper-pair density wave in $\text{Bi}_2\text{Sr}_2\text{CaCu}_2\text{O}_{8+x}$ *Nature* **532** 343
- [77] Choubey P *et al.* 2020 Atomic-scale electronic structure of the cuprate pair density wave state coexisting with superconductivity *Proc. Natl. Acad. Sci. USA* **117** 14805
- [78] Agterberg D F, Séamus Davis J C, Edkins S D, Fradkin E, Van Harlingen D J, Kivelson S A, Lee P A, Radzihovsky L, Tranquada J M, Wang Y 2020 The Physics of Pair-Density Waves: Cuprate Superconductors and Beyond *Annu. Rev. Condens. Matter Phys.* **11** 231
- [79] Sakurai Y *et al.* 2011 Imaging Doped Holes in a Cuprate Superconductor with High-Resolution Compton Scattering *Science* **332** 698
- [80] Hardy F, Hillier N J, Meingast C, Colson D, Li Y, Barišić N, Yu G, Zhao X, Greven M and Schilling J S 2010 Enhancement of the Critical Temperature of $\text{HgBa}_2\text{CuO}_{4+\delta}$ by Applying Uniaxial and Hydrostatic Pressure: Implications for a Universal Trend in Cuprate Superconductors *Phys. Rev. Lett.* **105** 167002
- [81] Wakimoto S, Birgeneau R J, Kagedan A, Kim H, Swainson I, Yamada K and Zhang H 2005 Magnetic properties of the overdoped superconductor $\text{La}_{2-x}\text{Sr}_x\text{CuO}_4$ with and without Zn impurities *Phys. Rev. B* **72** 064521
- [82] Kurashima K *et al.* 2018 Development of Ferromagnetic Fluctuations in Heavily Overdoped $(\text{Bi,Pb})_2\text{Sr}_2\text{CuO}_{6+\delta}$ Copper Oxides *Phys. Rev. Lett.* **121** 057002
- [83] Komiyama Y, Onishi S, Harada M, Kuwahara H, Kuroe H, Kurashima K, Kawamata T, Koike Y, Watanabe I and Adachi T 2021 Magnetic Impurity Effects on Ferromagnetic Fluctuations in Heavily Overdoped $(\text{Bi,Pb})_2\text{Sr}_2\text{Cu}_{1-y}\text{Fe}_y\text{O}_{6+\delta}$ Cuprates *J. Phys. Soc. Jpn.* **90** 084701
- [84] Sonier J E, Kaiser C V, Pacradouni V, Sabok-Sayr S A, Cochrane C, MacLaughlin D E, Komiya S and Hussey N E 2010 Direct search for a ferromagnetic phase in a heavily overdoped nonsuperconducting copper oxide *Proc. Natl. Acad. Sci. USA* **107** 17131
- [85] Kopp A, Ghosal A and Chakravarty S 2007 Competing ferromagnetism in high-temperature copper oxide superconductors *Proc. Natl. Acad. Sci. USA* **104** 6123
- [86] Barbiellini B and Jarlborg T 2008 Importance of Local Band Effects for Ferromagnetism in Hole-Doped La_2CuO_4 Cuprate Superconductors *Phys. Rev. Lett.* **101** 157002
- [87] Jia C J, Nowadnick E A, Wohlfeld K, Kung Y F, Chen C-C, Johnston S, Tohyama T, Moritz B and Devereaux T P 2014 Persistent spin excitations in doped antiferromagnets revealed by resonant inelastic light scattering *Nat. Commun.* **5** 3314
- [88] Maier T A and Scalapino D J 2020 Disappearance of Superconductivity in the Overdoped Cuprates *J. Supercond. Novel Magn.* **33** 15
- [89] Teranishi S, Nishiguchi K, Yunoki S and Kusakabe K 2021 Effect of On-site Coulomb Repulsion on Ferromagnetic Fluctuations in Heavily Overdoped Cuprates *J. Phys. Soc. Jpn.* **90** 094707
- [90] Himeda A, Kato T and Ogata M 2002 Stripe States with Spatially Oscillating d -Wave Superconductivity in the Two-Dimensional t - t' - J Model *Phys. Rev. Lett.* **88** 117001